catalysts

MDPI

Article

Characteristics of Vanadium-Based Coal Gasification Slag and the NH_3-Selective Catalytic Reduction of NO

Fang Han [1], Yanchun Gao [1], Qihuang Huo [1], Lina Han [2], Jiancheng Wang [1,*], Weiren Bao [1] and Liping Chang [1]

[1] State Key Laboratory Breeding Base of Coal Science and Technology Co-founded by Shanxi Province and the Ministry of Science and Technology, Taiyuan University of Technology, Taiyuan 030024, China; hanfang0802@163.com (F.H.); gaoyanchun7519@163.com (Y.G.); hqh102074311@163.com (Q.H.); baoweiren@tyut.edu.cn (W.B.); lpchang@tyut.edu.cn (L.C.)

[2] College of Materials Science and Engineering, Taiyuan University of Technology, Taiyuan 030024, China; hanlina@tyut.edu.cn

* Correspondence: wangjiancheng@tyut.edu.cn; Tel.: +86-138-3462-9730

Received: 8 July 2018; Accepted: 4 August 2018; Published: 9 August 2018

Abstract: In order to realize the resource utilization of coal gasification slag (CGS) and to effectively control the emission of nitrogen oxides (NO_x) in coke oven gas, the effect of the reaction conditions and vanadium loading over the CGS catalysts was carried out for the selective catalytic reduction (SCR) of NO by NH_3. The various vanadium loaded CGS catalysts were prepared using impregnation methods. The addition of 1% vanadium to the CGS catalyst (V1/CGS) significantly enhanced the NO conversion at a wide temperature range of 180–290 °C. The catalysts were characterized by N_2 adsorption/desorption, X-ray photoelectron spectroscopy, H_2-temperature programmed reduction, NH_3-temperature programmed desorption, Inductively coupled plasma optical emission spectrometer (ICP-OES), thermo gravimetric analyses (TGA), Fourier Transform infrared spectroscopy (FTIR), Scanning electron microscope-Energy dispersive spectrometer (SEM-EDS), and X-ray powder diffraction (XRD). The experimental results show the following: That (1) the NO removal efficiency of the sample CGS_3 was the best, and it could be up to 100% under the experimental conditions; (2) The NO removal efficiency of the catalysts was higher in the atmosphere with SO_2 than that without SO_2; (3) The XRD results indicated the active component of vanadium was homogeneously dispersed over CGS and the active component of catalyst was V_2O_5 according to the XPS results. In particular, the NH_3-TPD spectra of the vanadium loaded CGS catalyst showed that vanadium produced more acid sites, and the Lewis acid sites on the vanadium species were the active sites for the catalytic reduction of NO at 240–290 °C.

Keywords: coal gasification slag; NH_3-SCR; coke oven gas

1. Introduction

The coking chemical industry is an important part of the coal industry. However, the nitrogen oxides emitted from coke oven flue gas pollute our living environment and endanger our physical health. Therefore, the coking industry's flue gas treatment is imminent. According to reports, NH_3-selective catalytic reduction (SCR) technology is the most effective technology for removing NO_x from flue gases [1,2]. The commonly adopted commercial catalyst is V_2O_5–$WO_3(MoO_3)/TiO_2$ [2–4], and its working temperature must be above 300 °C in order to obtain good catalytic activity and to avoid pore plugging caused by the deposition of ammoniumsulfate salts over the catalyst surface. However, at low temperatures, the presence of H_2O and SO_2 can seriously affect SCR activity [5]. According to the

literature, some catalysts (such as MnO_2/Al_2O_3, CuO/AC (activated carbon), and Fe_2O_3/AC) show a high SCR activity at 120–250 °C, but they are prone to SO_2 deactivation because of the formation of sulfate salts [6–8]. Developing a catalyst that is resistant to SO_2 poisoning is critical to the SCR process. Studies have shown that in resisting the anti-ammonium sulfate, activated carbon or coke as a carrier is superior to TiO_2 and SiO_2 [9]. Zhu et al. [10] reported a carbon-supported vanadium oxide (V_2O_5/AC) catalyst for the SCR reduction. The catalytic activity was greatly promoted in the presence of SO_2. Numerous studies have reported that coal and coal-based materials (e.g., coal fly ash) could be prepared for activated carbons [11,12]. So, from the perspective of simplifying the process and saving costs, can we use coal gasification slag (CGS) as an alternative activated carbon for NO removal?

CGSs are solid by-products of the coal gasification process, including coarse slag (slags from lock hopper) and fine slag (slags from filter). They contain rich silica, alumina, and iron oxide as well as calcium oxide, magnesium oxide, titanium dioxide, and other inorganic materials. Recently, there have been some studies regarding the properties and applications of CGSs. Acosta et al. [13] used a 50% of lowcarbon coal gasification slag (burning loss rate only 2.64%) and clay to prepare the building bricks. Acosta et al. [14] found that the gas installations of a combined cycle (GICC) slag can be used as a raw material to produce glass fibers, glass ceramics, and ceramic sintered materials, in principle. However, most of the CGS is generally stored or placed in landfills, resulting in a waste of resources and pollution of the surrounding environment. Considering the similar properties of the CGS and coal-based materials, can coal gasification slag be high valued-added when used as an alternative source of activated carbon? For example, highly porous activated carbons were prepared from a coal gasification slag (CGS) precursor, and Pb^{2+} was removed from aqueous solution by KOH activation [15]. However, few studies have focused on using CGS to remove NO_x in flue gas.

In this study, CGS was used as a carrier and a V/CGS catalyst was prepared by pore volume impregnation. The SCR experiments were carried out by using a fixed bed reactor. The effects of the vanadium loading, temperature, and atmosphere on the NO removal activity of catalyst were investigated. The feasibility of using the gasified slag as the support for the SCR of NO by NH_3 was discussed.

2. Results and Discussion

2.1. Effect of Carrier

Figure 1 shows that the NO conversions increases with the increase of temperature, and the NO conversion of the catalyst is close to 100% in the temperature range of 260–290 °C. In the range of 180–260 °C, $V1/CGS_3$ shows a relatively higher $DeNO_x$ activity than $V1/CGS_1$ and $V1/CGS_2$, which may be due to the physical properties of $V1/CGS_3$ catalyst (see Table 1). Therefore, CGS_3 was used as the support in the following experiments. Figure 2 shows the N_2O formation and N_2 selectivity experiment of the $V1/CGS_3$ catalyst. Clearly, the N_2O formation slightly increases with an increase in temperature. Moreover, the N_2 selectivity of the $V1/CGS_3$ catalyst is always above 97% during the reaction, indicating that the catalyst has a good selectivity.

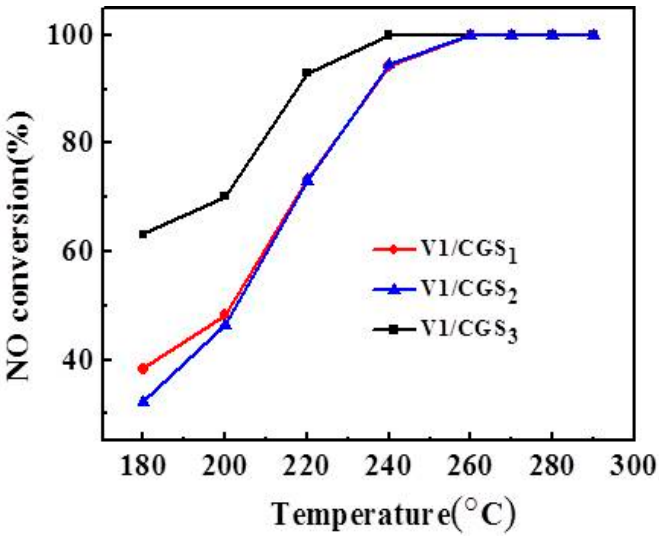

Figure 1. NO conversion of catalysts with different carriers.

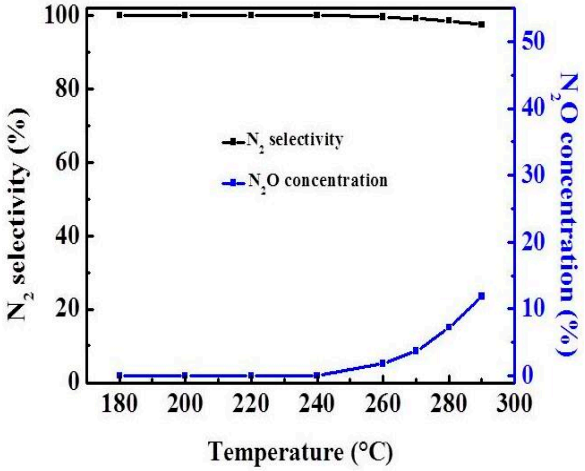

Figure 2. N_2O formation and N_2 selectivity for experiments of $V1/CGS_3$.

2.2. Effect of V Loading

Figure 3 shows the NO conversion curves over CGS_3 modified with different amounts of V_2O_5. Compared with the raw CGS_3, the NO reduction efficiencies of the V/CGSs are observed to be higher. S. Hums et al. [16] agrees that V_2O_5 could be more active than other vanadium species such as vavadates or polivanadates. The CGS activities are quite low in the reaction temperature. After the temperature reached 260 °C, the NO conversion rate decreased. But, the activity of the catalyst changed greatly when adding vanadium to the CGS. These results indicate that V loading is crucial to the SCR reaction. Moreover, it can be observed that the $V0.8/CGS_3$ catalyst activity is lower than that of the $V1/CGS_3$ catalyst, which may be due to the difference in the amount of V on the carrier. Adding litter vanadium to the catalyst does not influence the activity. However, when the content of V_2O_5 continues to increase, the catalyst activity decreased remarkably. At a certain temperature, the NO conversions over the $V1/CGS_3$ catalysts are in the following order of increasing: 7 wt%–3 wt%–1 wt%. It is possible that when the amount of V is lower, the vanadium active site on the catalyst surface is less. In addition, less SO_2 is adsorbed on the surface and less ammonium sulfate is formed on the surface of the catalyst, thus the activity is higher. Huang Zhanggen et al. [17] showed that the V_2O_5/AC catalyst activity can be enhanced by the large specific surface area activated coke carrier, because of the NH_3

adsorption and the dispersion of V_2O_5 on the catalyst. Figure 4 shows the Brunner-Emmet-Teller (BET) specific surface area of different samples, and it can be seen that the BET specific surface area of the V1/CGS_3 catalyst is larger than the other catalysts. In addition, the specific surface area of the V1/CGS_3 catalyst is slightly higher than that of the carrier. On the one hand, the difference is caused by the uneven distribution of CGS_3 itself. On the other hand, the difference in data may be caused by certain experimental errors, such as the error of sampling and weighing the sample. Of course, the surface area was not the determining factor for the SCR activity. In a word, considering the effects of the V loading on the NO removal rate of the V/CGS_3 catalyst, the suitable V loading is 1 wt%.

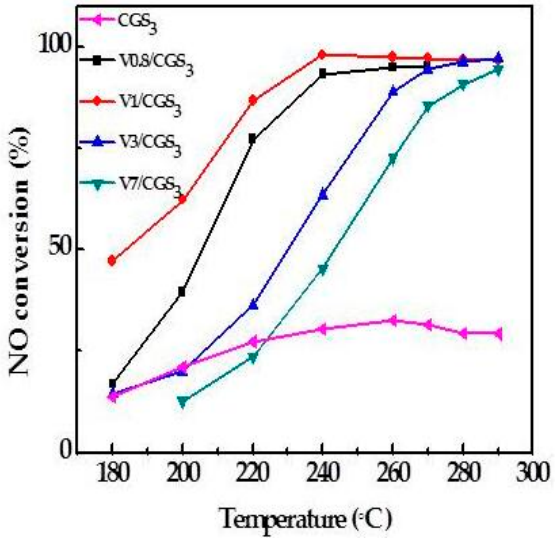

Figure 3. NO conversion of catalysts with different V loadings.

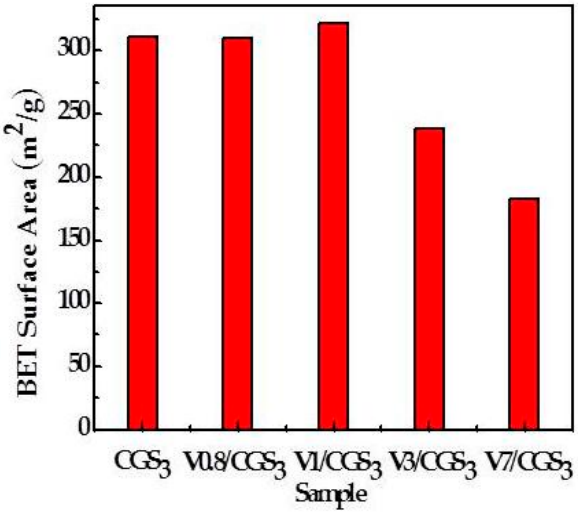

Figure 4. Surface areas of samples.

2.3. Effect of Atmosphere

As is known to all, the content of O_2 and H_2O in flue gas is much higher than that of SO_2 and NO, and the literature indicates that O_2 and H_2O have an effect on catalytic activity [1,18]. So, the effects of O_2 and H_2O on DeNO$_x$ activity were investigated using transient response technology, as shown in Figure 5. In stage one, the NO conversion stabilized at about 95% under all of the atmosphere conditions. But in stage two, when the O_2 was cut off and N_2 was added to keep the total flow

rate unchanged, the NO conversion rate decreased sharply, indicating that the SCR reaction mainly consumed gaseous O_2. In stage three, O_2 was added to make the atmosphere composition the same as that in stage one, and the catalytic activity was quickly restored. The NO conversion of stage four (cutting off the water in the atmosphere) is basically the same as stage five (adding to water), maintaining 100%. It indicated that a smaller amount of H_2O has no effect on catalytic activity at 260 °C, which is different from the conclusion that water will inhibit and poison the catalyst under the condition of SO_2 [5,19–21]. In stage six, the NH_3 was cut off, and N_2 was added to keep the total flow rate unchanged. At this time, the NO conversion gradually decreased to 16%. After the recovery of NH_3 in stage seven, the NO conversion increased rapidly to 95%. According to the phenomenon of stage six and stage seven, the main substance is the adsorptive NH_3 involved in the SCR reaction. Hence, it can be seen that O_2 and NH_3 are crucial in the process of SCR.

As can be seen from Figure 5, O_2 is crucial in the NH_3-SCR process, but how much O_2 is required to ensure the reaction? Different concentrations of O_2 were investigated, as shown in Figure 6. When the O_2 content was 1.9%, the NO conversion was stable at about 90% after 60 min. When the O_2 concentrations were 3.8% and 5.9%, respectively, the NO conversion curves basically coincided, indicating that the activity did not change with the O_2 concentration during the NH_3-SCR process. Therefore, the oxygen content under the experimental conditions is sufficient for the SCR reaction.

Transient response experiments revealed that H_2O had no significant effect on the activity at 260 °C. To further explore the effect of H_2O and SO_2 on the $DeNO_x$ activity, a temperature-programming experiment was designed. The results are shown in Figure 7. When H_2O was added to the reactant gas, the NO conversion rose slowly and eventually reached 60%, while over 60% was reached in absence of H_2O. This phenomenon is well documented in the literature on Mn-based catalysts [22] as a result of the competitive adsorption of H_2O and NH_3. Moreover, it also can be seen from Figure 7 that the NO conversion is the best in the presence of SO_2, reaching 100% at 240–290 °C. This result agrees with the XPS analysis, where the SO_2 promotion was attributed to the formation of SO_4^{2-} on the catalyst surface, which increased the NH_3 adsorption and promoted the NH_3 reaction with NO. However, the NO conversion decreased sharply when the reaction temperature is lower than 220 °C in the presence of SO_2 and H_2O. Zhu et al. [10] has reported that there was higher activity over the V_2O_5/AC catalyst when SO_2 was present in the reactant gas mixture. They believe that the reason is the formation of sulphate species on the catalyst surface. In summary, catalytic activity was promoted by SO_2. The possible reason is that V_2O_5 provides the adsorption and oxidation sites for SO_2, and increases the acidity, thus promoting the catalyst activity.

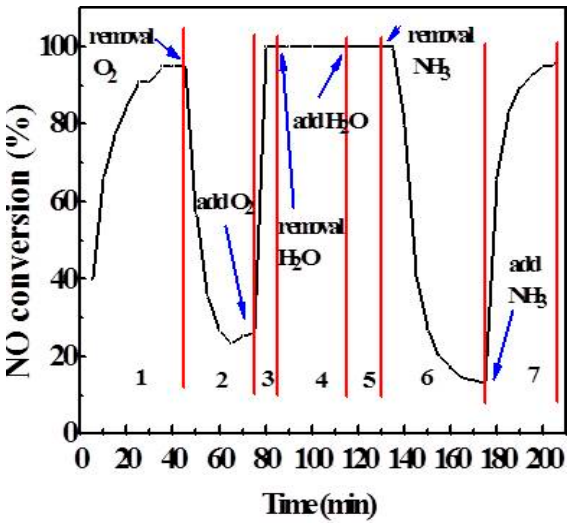

Figure 5. Effect of H_2O and O_2 on NO conversion.

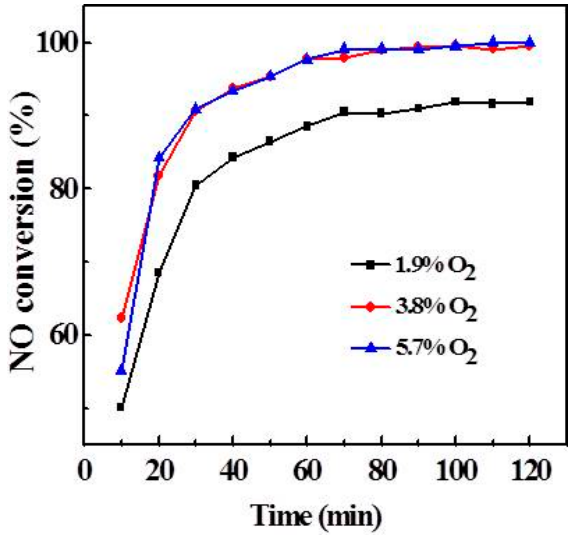

Figure 6. Effect of O_2 concentration on NO conversion.

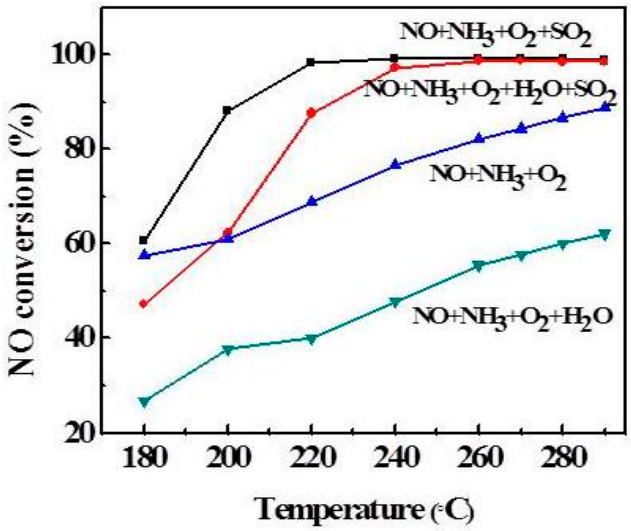

Figure 7. Effect of H_2O and SO_2 on NO conversion over V1/CGS_3 catalyst.

2.4. Effect of Reaction Temperature

As shown in Figure 3, 240–290 °C is the optimum temperature for the catalyst, and the NO conversion increases with the increasing reaction temperature, and the NO conversion is up to 95% at 240 °C. The effect of temperature on the SCR activity is that the increase of temperature will increase the thermal reaction of the molecules, and more molecules will reach the activated state, thereby improving the NO conversion. Moreover, the stability of the V1/CGS_3 catalyst experiment was investigated, as shown in Figure 8. The results showed that the NO conversion was maintained at 100% within 30 h of continuous testing at 260 °C. It shows that the catalyst exhibits a better stability.

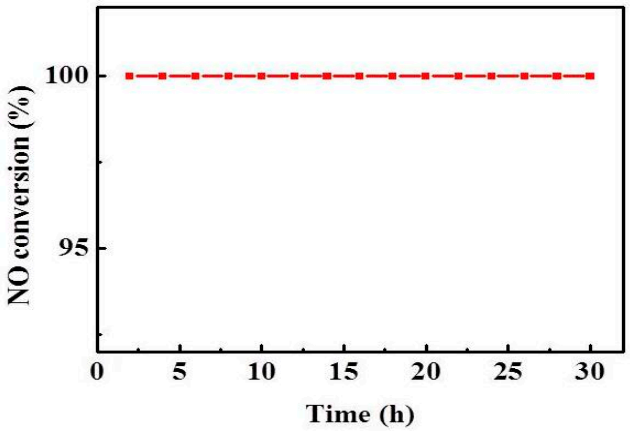

Figure 8. Stability of V1/CGS_3 catalyst.

2.5. The Physical Properties of CGS

When the V/CGS catalyst is used for the reduction of NO by NH_3, the catalytic activity is affected by the specific surface area of the carrier. For this purpose, three different gasification slags were selected to prepare the V1/CGS catalyst, so as to select the best active gasification residue carrier. The surface area and pore structure of the catalysts are listed in Table 1. It can be seen that the BET surface areas and mesopore volumes of CGS_3 are between the CGS_1 and CGS_2 carrier, but its micro-pore area is higher than the other two CGSs, by up to 111 m^2/g. It can be seen that after loading vanadium, the BET areas and micro-pore volumes of the catalysts are increased slightly. According to the literature, the conversion rate of NO can be improved to a certain extent by micropore and mesoporous; the micro-pores were conducive to the dispersion of the active component and the mesopores ensured that the reactants can enter to the interior of the AC [23,24]. In the study, the addition of vanadium to the CGS catalyst led to new micro-pores and mesopores, thus improving the NO conversion (shown in Figure 3). Moreover, after the reaction, the BET surface areas and micropore volumes of V1/CGS_3 decreased significantly. The results suggested that the ammonium sulfate salts or H_2SO_4 may have formed during the SCR reaction, or indicated that a large amount of material was generated in the reaction, blocking the channel [25].

Table 1. Physical property of the coal gasification slags (CGSs) and V1/CGS Catalysts.

Samples	BET Surface Area (m^2/g)	Micro-Pore Area (m^2/g)	Mesopore Volume (cm^3/g)	Micro-Pore Volume (cm^3/g)
CGS_1	212.8	94.5	0.13	0.04
CGS_2	318.7	93.1	0.27	0.04
CGS_3	311.4	111.0	0.18	0.05
V1/CGS_3 fresh	321.5	115.6	0.19	0.05
V1/CGS_3 used	203.5	61.2	0.15	0.03

Table 2 presents the ash analyses of the CGSs' catalyst. The samples were calcined at a high temperature and then digested with concentrated acid. Finally, the element analysis was carried out using ICP. There are mainly SiO_2, CaO, Fe_2O_3, and Al_2O_3 in the ash. SiO_2 is often taken as a catalyst support, and it is advantageous for the SCR reaction. Of course, Al_2O_3 has been widely used as a carrier in the field of catalysis because of its pore structure, surface acidity, and other properties [26,27]. It has been reported that CaO can deactivate the SCR catalyst because it interacts with the active component V_2O_5, thereby reducing the acidity and reducibility of the catalyst surface [28,29]. However, CaO has a certain desulfurization activity. Ma et al. [30] used activated coke, prepared from semicoke through steam, to support Ca for the flue gas SO_2 removal. Ca/AC showed a high SO_2 removal capacity. Moreover, Fe_2O_3 is taken as a support for removing Hg. For example, Yang et al. [31] used Mn/γ-Fe_2O_3

magnetic adsorbents to remove the elemental mercury from the flue gas. In the present study, Fe_2O_3 has a slight effect on the SCR reaction. Moreover, Li et al. [32] reported that although the total contents of the ashes in the ACs were equal to or higher than the V_2O_5 loadings in the catalysts, the ashes cannot interfere with the catalytic activity of V_2O_5. In a word, it can be seen from Table 2 that the ash content of CGS_3 is less than that of other gasification slags, indicating that its carbon skeleton structure plays a major role and provides a specific surface area and pores.

Table 2. Elemental analysis of CGS_3 and $V1/CGS_3$ catalyst.

Samples	Composition (wt %)						
	SiO_2	Fe_2O_3	CaO	Al_2O_3	Na_2O	TiO_2	V_2O_5
CGS_1	14.5	20.0	7.9	3.9	0.8	0.2	0
CGS_2	12.8	6.4	5.1	5.1	0.8	0.2	0
CGS_3	11.9	3.0	2.9	3.1	0.5	0.1	0
$V1/CGS_3$ fresh	8.9	2.9	2.6	2.6	0.4	0.1	1.3
$V1/CGS_3$ used	7.4	2.5	3.0	2.3	0.3	0.1	1.0

2.6. Thermo Gravimetric (TG) and Derivative Thermo Gravimetric (DTG

As Figure 9 shows, it was obvious that the mass of the CGSs began to significantly decline at 470 °C, and the weight losses of the CGSs were different, for which CGS_2 was 50% and CGS_3 was 54%. The departure of the water molecules and hydration may be responsible for this phenomenon. In a word, it can also indicate that the gasification slag has a certain stability under the experimental temperature.

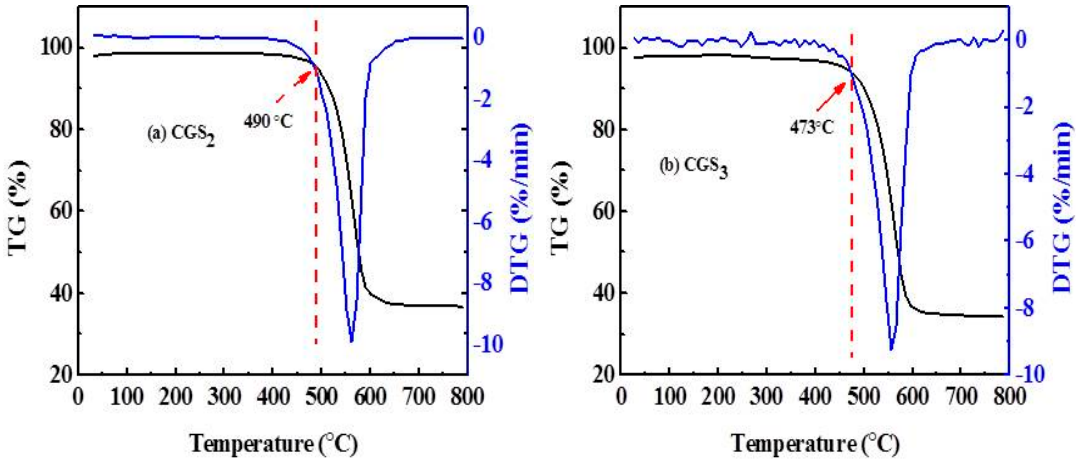

Figure 9. Thermo gravimetric (TG) and Derivative Thermo Gravimetric (DTG) profiles of the (**a**) CGS_2 and (**b**) CGS_3.

2.7. XRD

The XRD patterns of the catalyst samples are depicted in Figure 10. It was observed that all of the samples show two broad peaks at 25° and 43°. These peaks could be ascribed to the diffraction of the graphite (002) and (100) crystal planes, respectively [33]. It also showed that the other peaks of patterns were ascribed to the SiO_2 and $CaCO_3$. For the CGS_3 and $V1/CGS_3$ peaks, the intensity and peak width were almost same. Moreover, with the increase of V loading (1%–7%), the intensity and width of the peak becomes weak, but the diffraction peaks attributed to the V species were not observed, suggesting that the loaded active phase was highly dispersed on the CGS support, so that the catalytic activity improved, as shown in Figure 3.

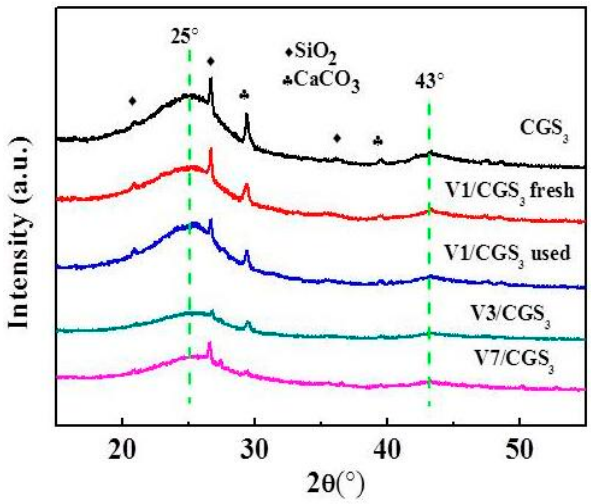

Figure 10. X-ray diffraction (XRD) patterns of catalysts.

2.8. XPS

In order to investigate the chemical information of $V1/CGS_3$ surface, the surface binding energies and valence states of the various catalyst materials were studied using XPS analysis. The results are shown in Figure 11. The XPS spectrogram of the sample 505–530 eV is shown in Figure 11a. According to the V 2p photoelectron peak, the peak at 516.4–517.0 eV was assigned to V^{5+}, the peak at 515.7–516.2 eV was ascribed to V^{4+} [34], and the peak at 513.1–514.7 eV was assigned to V^{3+} [35], respectively. V^{5+} is a stable oxidation state and has an important influence on the catalyst activity. In Figure 11a, it can be discerned that the V $2P_{3/2}$ peak at 517.2 eV in the fresh catalyst is ascribed to V^{5+}, and in the used catalyst, there is a new peak at 516.3 eV ascribed to V^{4+}, which indicates a partial reduction of V^{5+} to the lower-valence V^{4+}, and there may be V_2O_4 or $VOSO_4$ on the used catalyst surface, except for V_2O_5. In the $SP_{3/2}$ spectrum, as shown in Figure 11b, no peaks were observed on the fresh catalyst. In adition, the $SP_{3/2}$ spectrum of the used catalyst was composed of two peaks at 168.5 and 169.2 eV. The peak at 168.5 eV is attributed to the S^{6+} species. It may confirm the formation of a small amount of $VOSO_4$ during the activity test. The last peak may correspond to H_2SO_4, because the peak at 169.7 eV was assigned to H_2SO_4 in the literature [36]. At present, it is not clear what caused the peak deviation.

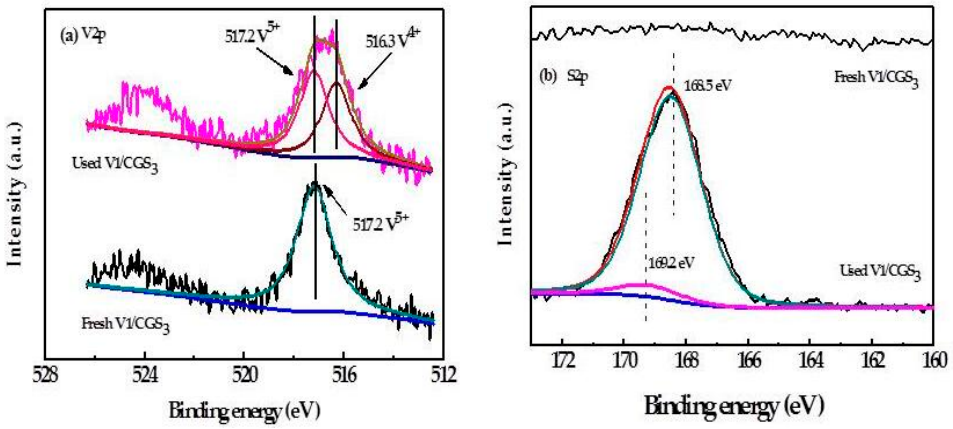

Figure 11. X-ray photoelectron spectrometry (XPS) spectra of (**a**) V2p and (**b**) S2p for the fresh and used $V1/CGS_3$.

2.9. FTIR

Figure 12 shows the FTIR spectra of the V1/CGS_3 before and after the SCR reaction in the presence of H_2O and SO_2. There is a broad band at 1000–1220 cm^{-1} attributed to the V^{5+}=O stretching vibration in V_2O_5/AC, which is stronger than the fresh catalyst [37]. The phenomenon shows that the symmetry of the vanadium species is higher than that of the fresh catalyst. The bands at 1104 and 668 cm^{-1} may be the vibration of the SO_4^{2-} ions. The SO_4^{2-} ions show two infrared peak at 1104 (ν_1) and 613 (ν_2) [4]. The band around 1460 cm^{-1} was assigned to the symmetrical bending vibrations of the NH^{4+} species [38]. Leo et al. [39] showed that the band at 1000 cm^{-1} was due to the V–O stretching vibration peak of $VOSO_4$. Hwever, Raziyeh et al. [40] showed that the bands at 1410 cm^{-1} and 1150 cm^{-1} were attributed to $VOSO_4$, which may be due to the influence of the carrier carbon changing its symmetry. Therefore, the 1400 cm^{-1} band is attributed to the formation of $VOSO_4$. The catalyst after the SCR reaction is shown to contain SO_4^{2-} and NH_4^+ by FTIR, which suggests that the ammonium sulfate salts deposited on the catalyst surface during the SCR reaction.

Therefore, it can be seen from the XPS and FTIR results that H_2SO_4, ammonium sulfate, and $VOSO_4$ are formed on the surface after the NH_3-SCR reaction.

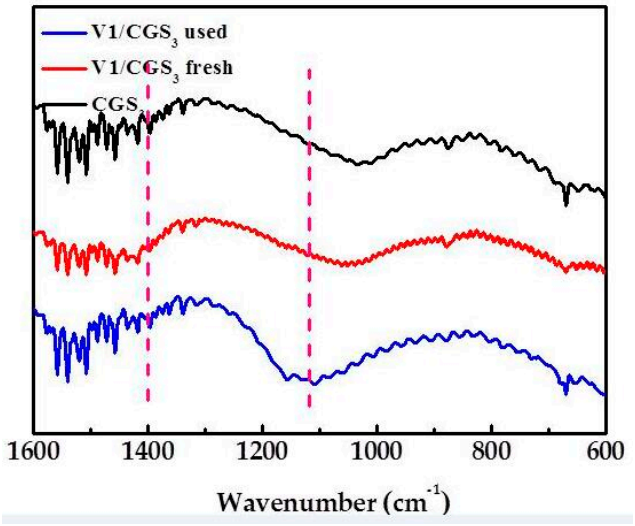

Figure 12. FTIR spectra of the fresh and used V1/CGS_3.

2.10. SEM-EDS

Figure 13 shows the EDS spectra of the vanadium distribution on different samples. It can be seen that by increasing the vanadium loading, the vanadium is more likely to aggregate together and is more compactly dispersed on the surface of the CGS_3. When the V loading is slightly higher, more active reaction sites can be provided for the SCR reaction. However, when the V loading is too high, the pores of the catalyst are blocked to some extent, and the specific surface area is lowered, which inhibits the SCR reaction. The results can be seen from Figures 3 and 4.

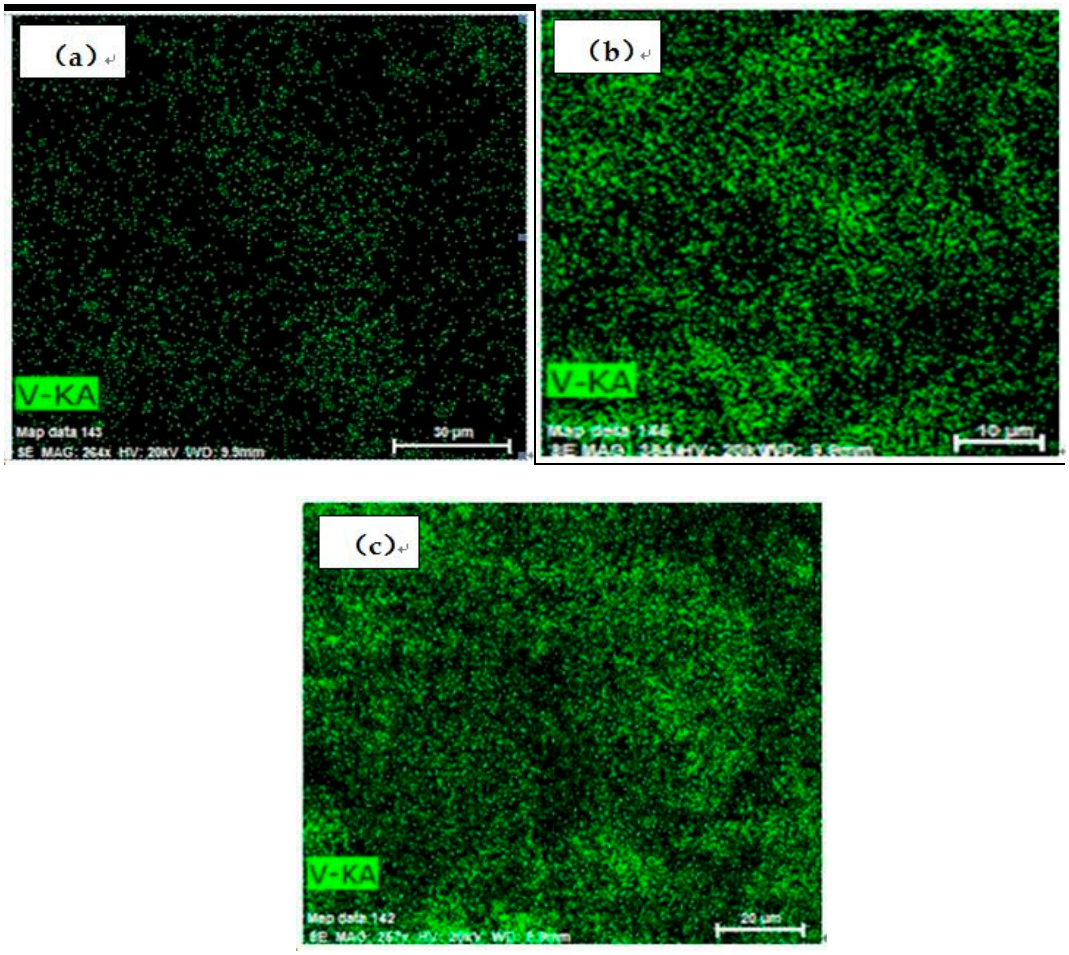

Figure 13. Surface characteristics of (**a**) V1/CGS_3; (**b**) V3/CGS_3; and (**c**) V7/CGS_3.

2.11. NH_3-TPD

TPD analysis, one of the most common techniques, was carried out to characterize the functional groups on the carbonaceous surfaces [41]. The acid strength in V1/CGS_3 was determined by NH_3-TPD. Figure 14 shows the NH_3-TPD profiles over CGS_1, CGS_2, CGS_3, V1/CGS_3, V3/CGS_3, and V7/CGS_3. It was observed that the V1/CGS_3 catalyst shows two types of acid sites, so NH_3 can be adsorbed on the catalyst. According to the authors of [42], it could be considered that the formation of a low-temperature peak was mainly attributed to the desorption of ammonia bound to weak Bronsted acid sites and physisorbed ammonia molecules, while the high-temperature maximum could be caused by the desorption of NH_3 from the Lewis acid sites. With the addition of V to the CGS support, the bound NH_3 absorption increased significantly, suggesting that V produced more acid sites for the catalyst. In particular, the vanadium species showed a significant adsorption ability toward NH_3 at the Lewis (L) acid sites. Huang et al. [43] found that the Lewis acid sites on the surface of the V_2O_5/CNT are the active sites in the process of NH_3-SCR at low temperatures. Moreover, it was clear that by increasing the vanadium loading (1%–7%), the peak intensity of the L acid site becomes weak. According to the EDS results, the more vanadium supported on the carrier, the easier it is to gather together. As a result, the effective active component of vanadium provided on the catalyst is reduced, thereby reducing the activity. This is the main reason that the activity is reduced when the amount of vanadium is increased. All in all, in connection with the catalytic activity, it is believed that the Lewis acid sites on the vanadium species were the active sites for the SCR of NO with NH_3 at 240–290 °C on the V1/CGS_3 catalyst.

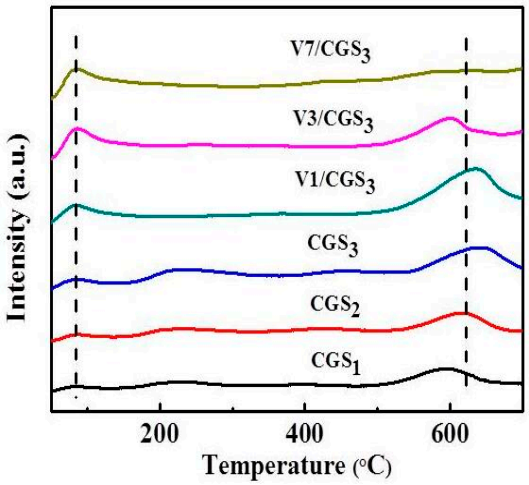

Figure 14. NH_3-temperature programmed desorption (TPD) patterns of catalysts.

2.12. H_2-TPR

The redox ability of the VO_x species was thought to be another key factor in the SCR process. Temperature program reduction (TPR) has become one of the techniques to characterize the reduction behaviors of the dispersed VO_x species. As shown in Figure 15, the CGS_1, CGS_2, and CGS_3 catalysts only showed one broad peak, which may be related to the nature of the gasification residue itself. With the introduction of V into the support, it was obviously observed that the $V1/CGS_3$ catalyst shows two redox peaks. The redox peaks in the range of 450–600 °C were assigned to the reduction of the VO_x monolayer species from V^{5+} to V^{3+} [44]. With the addition of vanadium, the redox peaks shifted to the lower temperature side, which could be due to a good dispersion of V.

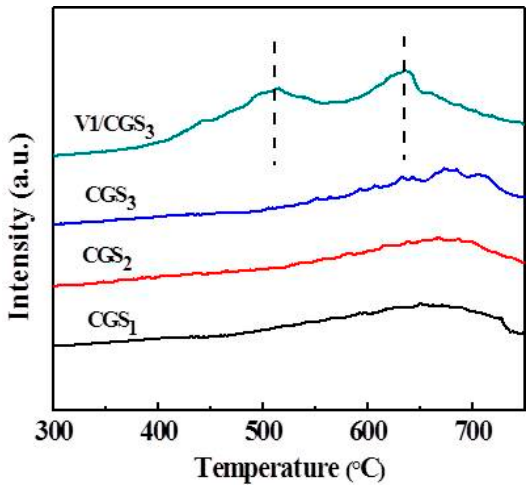

Figure 15. H_2-temperature programmed reduction (TPR) patterns of catalysts.

3. Materials and Methods

3.1. Preparation of Supports and Catalysts

Three gasification residues are chosen and labeled as CGS_1, CGS_2, and CGS_3 (China), respectively. The CGS was grounded to 40–60 mesh, and a V/CGS catalyst was prepared using pore volume impregnation [5]. The vanadium oxide was supported on the CGS with an aqueous of ammonium meta-vanadate (Tianjin, China, 99%) in oxalic acid (Tianjin, China, 99%). The V loading in the catalysts

were determined by the concentration of the ammonium meta-vanadate used in the impregnation. After the impregnation, the catalyst was dried at 50 °C and then 120 °C for 5 h, and subsequently calcined in N_2 for 5 h at 500 °C and pre-oxidized in air at 250 °C for 5 h.

3.2. Catalytic Activity Test

The SCR activity measurement was conducted in a fixed-bed quartz reactor. Mass flow meters were used to control the flow rate. The catalyst was placed in the middle of the reactor (D24 × 50 mm) and heated to the experimental temperature in the atmosphere of N_2, and then passed into the simulated flue gas and the reducing agent, NH_3. To prevent the formation of ammonium sulfate salts [1] in the inlet tubing of the reactor, the gases were sent to the buffer bottle fully mixed before entering the reaction tube. The simulated flue gas composition was as follows: 500 ppm NO, 500 ppm NH_3, 200 ppm SO_2 (when used), 3 vol% H_2O (when used), and 6 vol% O_2, and the balance gas that was used was N_2. In all of the runs, the total gas flow rate was maintained at 400 mL/min. The concentration of the inlet and outlet NO was simultaneously measured usng an on-line Flue Gas Analyzer (KM9106) equipped with an NO sensor. The NO conversion was calculated using the formula given below.

$$\eta_{NO} = \frac{C_{NO,in} - C_{NO,out}}{C_{NO,out}} \times 100\% \quad (1)$$

$$S_{N2} = \frac{C_{NO,in} + C_{NH_3,in} - C_{NO_2,out} - 2 \times C_{N_2O,out}}{C_{NO,in} + C_{NH_3,in}} \times 100\% \quad (2)$$

where η_{NO} is the NO conversion, and $C_{NO,in}$ and $C_{NO,out}$ are the NO concentrations in the inlet and outlet gas, as measured by a flue gas analyzer, respectively. S_{N2} is the N_2 selectivity, C_{NO_2}, out is the N_{O_2} concentration in the outlet gas, $C_{N_2O,out}$ is the N_2O concentration in the outlet gas, and $C_{NH_3,in}$ is the NH_3 concentration in the inlet gas.

3.3. Catalysts Characterization

The specific surface area and pore structure parameters of the catalysts were determined using the nitrogen physical adsorption instrument (Micromeritics, Norcross, GA, USA). The inductively coupled plasma optical emission spectrometer (ICP-OES) (SPECTRO, Kleve, Germany) was used to analyze the ash contents of the catalysts. The surface element valence of the sample was analyzed by X-ray photoelectron spectroscopy (Thermo Fisher Scientific, Waltham, MA, USA). The structural characterizations of the catalysts were analyzed using X-ray powder diffraction (XRD) (Rigaku, Tokyo, Japan). The diffraction patterns were scanned in the 2θ range from 10° to 70° at the scanning rate of 5°/min. The thermo gravimetric analyses (TGA) were performed with a NETZSCH Thermal Analysis System to study the catalyst stability (NETZSCH Corporation, Bavaria, Germany). The Fourier Transform infrared spectroscopy (FTIR) spectra were collected on a Bruker TENSOR 27 (Bruker Corporation, Karlsruhe, Germany). The surface morphology of the samples was studied by field-emission scanning electron microscopy (SEM) (JEOL, Tokyo, Japan), combined with an energy dispersive spectrometer (EDS) (Bruker, Karlsruhe, Germany).

Temperature program reduction (TPR) and temperature programmed desorption (TPD) tests were carried out on the AutoChem II type high performance chemical adsorption instrument (Micromeritics, Norcross, GA, USA). The 150 mg samples were dried at 150 °C for 30 min in Ar (30 mL/min), and cooled to 50 °C. Then, the sample was heated up to 800 °C at a 10 °C/min rate in 10% H_2/Ar atmosphere. For NH_3-TPD, the 150 mg samples were pretreated in carrier gas for 30 min at 150 °C, and then exposed to 10% NH_3/He (30 mL/min) at 50 °C for 30 min, followed by a temperature ramp to 700 °C at a rate of 10 °C/min; the concentration of desorbed NH_3 was determined by the thermal conductivity detector.

4. Conclusions

In this work, the SCR activity and physicochemical properties of the V/CGS catalyst have been investigated. The results showed that the prepared catalyst in the 240–290 °C temperature range showed good catalytic activity. The high-carbon content gasification slag has a developed pore structure and is similar to the structure of activated carbon made of coal. The active metal vanadium shows good activity, and the main active component for $DeNO_x$ of V1/CGS catalyst is V_2O_5; the V1/CGS catalyst impregnated with 1 wt% vanadium has the best $DeNO_x$ activity; and the NO conversion increases from 60% to 100% with the increasing temperature (200–250 °C). The vanadium loaded CGS catalyst showed that vanadium gave rise to more acid sites for the catalyst, and the Lewis acid sites on the vanadium species were the active sites for catalytic reduction of NO, and the certain sulfur-resistance ability over V/CGS is shown. The above results indicate that the gasification slag can be used as a carrier to prepare a carbon-based catalyst for the NO_x removal from the flue gas. The simultaneous removal of SO_2, NO_x, and Hg over this catalyst will be studied in our future work.

Author Contributions: The experimental work was conceived and designed by F.H. and J.W; F.H. and Y.G. performed the experiments; F.H. and Q.H. analyzed the date; and F.H. drafted the paper. The manuscript was amended through the comments of W.B., L.C., L.H, and J.W. All of the authors have given approval for the final version of the manuscript.

Acknowledgments: This work was supported by the National Natural Science Foundation of China (21476154), the Shanxi Province Natural Science Foundation (201601D011083), the Research Project Supported by Shanxi Scholarship Council of China (2016-026), and the State Key Laboratory of Coal Combustion (FSKLCCA1606).

Conflicts of Interest: The authors declare no conflict of interest.

References

1. Bosch, H.; Janssen, F. Formation and control of nitrogen oxides. *Catal. Today* **1988**, *2*, 369–379.
2. Cho, S.M. Properly apply selective catalytic reduction for NO_x removal. *Chem. Eng. Prog.* **1994**, *90*, 39–45.
3. Chen, J.P.; Yang, R.T. Mechanism of poisoning of the V_2O_5/TiO_2 catalyst for the reduction of NO by NH_3. *J. Catal.* **1990**, *125*, 411–420. [CrossRef]
4. Chen, J.P.; Yang, R.T. Selective catalytic reduction of NO with NH_3 on SO_4^{2-}/TiO_2 superacid catalyst. *J. Catal.* **1993**, *139*, 277–288. [CrossRef]
5. Huang, Z.; Zhu, Z.; Liu, Z. Combined effect of H_2O and SO_2 on V_2O_5/AC catalysts for NO reduction with ammonia at lower temperatures. *Appl. Catal. B* **2002**, *39*, 361–368. [CrossRef]
6. Zhu, Z.; Hu, T. NO reduction with NH_3 over an activated carbon—supported copper oxide catalysts at low temperatures. *Appl. Catal. B* **2000**, *26*, 25–35. [CrossRef]
7. Singoredjo, L.; Korver, R.; Kapteijn, F.; Moulijn, J. Alumina supported manganese oxides for the low-temperature selective catalytic reduction of nitric oxide with ammonia. *Appl. Catal. B* **1992**, *24*, 297–316. [CrossRef]
8. Grzybek, T.; Papp, H. Cheminform abstract: Selective catalytic reduction of nitric oxide by ammonia on Fe^{3+}-promoted active carbon. *Appl. Catal. B* **1992**, *24*, 271–283. [CrossRef]
9. Zhu, Z.; Niu, H.; Liu, Z.; Liu, S. Decomposition and reactivity of NH_4HSO_4 on V_2O_5/AC catalysts used for NO reduction with ammonia. *J. Catal.* **2000**, *195*, 268–278. [CrossRef]
10. Zhu, Z.; Liu, Z.; Niu, H.; Liu, S. Promoting effect of SO_2 on activated carbon-supported vanadia catalyst for NO reduction by NH_3 at low temperatures. *J. Catal.* **1999**, *187*, 245–248. [CrossRef]
11. Lorenc-Grabowska, E.; Gryglewicz, G. Adsorption characteristics of congo red on coal-based mesoporous activated carbon. *Dyes Pigments* **2007**, *74*, 34–40. [CrossRef]
12. Rubio, B.; Izquierdo, M.T.; Mayoral, M.C.; Bona, M.T.; Andres, J.M. Unburnt carbon from coal fly ashes as a precursor of activated carbon for nitric oxide removal. *J. Hazard. Mater.* **2007**, *143*, 561–566. [CrossRef] [PubMed]
13. Acosta, A.; Iglesias, I.; Aineto, M.; Romero, M.; Rincón, J.M. Utilisation of igcc slag and clay steriles in soft mud bricks (by pressing) for use in building bricks manufacturing. *Waste Manag.* **2002**, *22*, 887–891. [CrossRef]

14. Acosta, A.; Aineto, M.; Iglesias, I.; Romero, M.; Rincón, J.M. Physico-chemical characterization of slag waste coming from gicc thermal power plant. *Mater. Lett.* **2001**, *50*, 246–250. [CrossRef]
15. Xu, Y.; Chai, X. Characterization of coal gasification slag based activated carbon and its potential application in lead removal. *Environ. Technol.* **2017**, *41*, 382–391. [CrossRef] [PubMed]
16. Hums, E. Is advanced scr technology at a standstill? A provocation for the academic community and catalyst manufacturers. *Catal. Today* **1998**, *42*, 25–35. [CrossRef]
17. Huang, Z.; Niu, H. Effect of activated coke property on V_2O_5/AC activity for reduction of NO in flue gas at low temperature. *Coal Convers.* **2001**, *24*, 74–78.
18. Davini, P. Adsorption and desorption of sulphur dioxide from simulated flue gas on active carbon: The effect of the ash content. *Carbon* **1993**, *31*, 47–51. [CrossRef]
19. Long, R.Q.; Yang, R.T. Superior Fe-ZSM-5 catalyst for selective catalytic reduction of nitric oxide by ammonia. *J. Am. Chem. Soc.* **1999**, *121*, 5595–5596. [CrossRef]
20. Long, R.Q.; Yang, R.T. Selective catalytic reduction of NO with ammonia over V_2O_5 doped TiO_2 pillared clay catalysts. *Appl. Catal. B* **2000**, *24*, 13–21. [CrossRef]
21. Long, R.Q.; Yang, R.T. Selective catalytic reduction of nitrogen oxides by ammonia over Fe^{3+}-exchanged TiO_2-pillared clay catalysts. *J. Catal.* **1999**, *186*, 254–268. [CrossRef]
22. Pan, S.; Luo, H.; Li, L.; Wei, Z.; Huang, B. H_2O and SO_2 deactivation mechanism of MnOx/MWCNTs for low-temperature SCR of NO_x with NH_3. *J. Mol. Catal. A-Chem.* **2013**, *377*, 154–161. [CrossRef]
23. Li, P.; Liu, Q.; Liu, Z. N_2O and CO_2 formation during selective catalytic reduction of NO with NH_3 over V_2O_5/AC catalyst. *Ind. Eng. Chem. Res.* **2011**, *50*, 341–350.
24. Boyano, A.; Gálvez, M.E.; Moliner, R.; Lázaro, M.J. Carbon-based catalytic briquettes for the reduction of NO: Effect of H_2SO_4 and HNO_3 carbon support treatment. *Fuel* **2008**, *87*, 2058–2068. [CrossRef]
25. Yang, W.; Liu, F.; Xie, L.; Lian, Z.; He, H. Effect of V_2O_5 additive on the SO_2 resistance of a Fe_2O_3/AC catalyst for NH_3-SCR of NO_x at low temperatures. *Ind. Eng. Chem. Res.* **2016**, *55*, 2677–2685. [CrossRef]
26. Potdar, H.S.; Jun, K.W.; Bae, J.W.; Kim, S.M.; Lee, Y.J. Synthesis of nano-sized porous γ-alumina powder via a precipitation/digestion route. *Appl. Cataly. A-Gen.* **2007**, *321*, 109–116. [CrossRef]
27. Parida, K.M.; Pradhan, A.C.; Das, J.; Sahu, N. Synthesis and characterization of nano-sized porous gamma-alumina by control precipitation method. *Mater. Chem. Phys.* **2009**, *113*, 244–248. [CrossRef]
28. Klimczak, M.; Kern, P.; Heinzelmann, T.; Lucas, M.; Claus, P. High-throughput study of the effects of inorganic additives and poisons on NH_3-SCR catalysts—Part I: V_2O_5-WO_3/TiO_2 catalysts. *Appl. Catal. B* **2010**, *95*, 39–47. [CrossRef]
29. Kröcher, O.; Elsener, M. Chemical deactivation of V_2O_5-WO_3/TiO_2 SCR catalysts by additives and impurities from fuels, lubrication oils, and urea solution: I. Catalytic studies. *Appl. Catal. B* **2008**, *77*, 215–227. [CrossRef]
30. Jianrong, M.; Mengxue, A. A novel Ca/AC desulphurizer. *Coal Convers.* **2001**, *24*, 48–53.
31. Yang, S.; Guo, Y.; Yan, N.; Qu, Z.; Xie, J.; Yang, C.; Jia, J. Capture of gaseous elemental mercury from flue gas using a magnetic and sulfur poisoning resistant sorbent Mn/γ-Fe_2O_3 at lower temperatures. *J. Hazard. Mater.* **2011**, *186*, 508–515. [CrossRef] [PubMed]
32. Li, P.; Liu, Z.; Li, Q.; Wu, W.; Liu, Q. Multiple roles of SO_2 in selective catalytic reduction of NO by NH_3 over V_2O_5/AC catalyst. *Ind. Eng. Chem. Res.* **2014**, *53*, 7910–7916. [CrossRef]
33. Liu, L.; Liu, Z.; Yang, J.; Huang, Z.; Liu, Z. Effect of preparation conditions on the properties of a coal-derived activated carbon honeycomb monolith. *Carbon* **2007**, *45*, 2836–2842. [CrossRef]
34. Xiao, Y.; Liu, Z.; Liu, Q.; Wang, J.; Xing, X.; Huang, Z. Mechanism of SO_2 influence on NO removal over V_2O_5/AC catalyst. *Chin. J. Catal.* **2008**, *29*, 81–85.
35. Seo, P.W.; Lee, J.Y.; Shim, K.S.; Hong, S.H.; Hong, S.C.; Hong, S.I. The control of valence state: How V/TiO_2 catalyst is hindering the deactivation using the mechanochemical method. *J. Hazard. Mater.* **2009**, *165*, 39–47. [CrossRef] [PubMed]
36. Wren, A.G.; Phillips, R.W.; Tolentino, L.U. Surface reactions of chlorine molecules and atoms with water and sulfuric acid at low temperatures. *J. Colloid Interface Sci.* **1979**, *70*, 544–557. [CrossRef]
37. Zhu, Z.; Liu, Z.; Niu, H.; Liu, S.; Hu, T.; Liu, T. Mechanism of SO_2 promotion for NO reduction with NH_3 over activaed carbon—Supported vanadium oxide catalyst. *J. Catal.* **2001**, *197*, 6–16. [CrossRef]
38. Pan, Y.; Zhao, W.; Zhong, Q.; Cai, W.; Li, H. Promotional effect of Si-doped V_2O_5/TiO_2 for selective catalytic reduction of NO_x by NH_3. *Acta Sci. Circumstantiae* **2013**, *25*, 1703–1711.

39. Frederickson, L.D.; Hausen, D.M. Infrared spectra-structure correlation study of vanadium-oxygen compounds. *Anal. Chem* **1963**, *35*, 818. [CrossRef]
40. Khodayari, R.; Odenbrand, C.U.I. Regeneration of commercial SCR catalysts by washing and sulphation: Effect of sulphate groups on the activity. *Appl. Catal. B* **2001**, *33*, 277–291. [CrossRef]
41. Zhuang, Q.; Kyotani, T.; Tomita, A. Drift and TK/TPD analyses of surface oxygen complexes formed during carbon gasification. *Energy Fuels* **1994**, *8*, 714–718. [CrossRef]
42. Niwa, M.; Habuta, Y.; Okumura, K.; Katada, N. Solid acidity of metal oxide monolayer and its role in catalytic reactions. *Catal. Today* **2003**, *87*, 213–218. [CrossRef]
43. Huang, B.; Huang, R.; Jin, D.; Ye, D. Low temperature scr of NO with NH_3 over carbon nanotubes supported vanadium oxides. *Catal. Today* **2007**, *126*, 279–283. [CrossRef]
44. Amiridis, M.D.; Wachs, I.E.; Deo, G.; Jehng, J.M.; Du, S.K. Reactivity of V_2O_5 catalysts for the selective catalytic reduction of NO by NH_3: Influence of vanadia loading, H_2O, and SO_2. *J. Catal.* **1996**, *161*, 247–253. [CrossRef]